Elsevier Editorial System(tm) for Journal of Terramechanics

Manuscript Draft

Manuscript Number: JTERRA-D-16-00057R1

Title: Thermal vision, moisture content, and vegetation in the context of off-road mobile robots

Article Type: Research Paper

Keywords: terrain traversability; terrain characterization; non-geometric hazards; thermal inertia; moisture meter; temperature probe.

Corresponding Author: Dr. Ramon Gonzalez, Ph.D.

Corresponding Author's Institution: Massachusetts Institute of Technology

First Author: Ramon Gonzalez, Ph.D.

Order of Authors: Ramon Gonzalez, Ph.D.; Alejandro Lopez, PhD; Karl Iagnemma, PhD

Abstract: This paper describes an initial investigation that shows the major impact that moisture and vegetation produce on a soil and how that effect may be measured using a thermal camera. In particular, those two variables influence how the soil compacts and, hence, the traversability of a vehicle. A broad set of experiments, under different weather conditions and with different soils, demonstrate that thermal properties derived from the thermal camera (i.e. thermal inertia) increase when moisture content of sandy soils increases. In addition to that, a relation is observed between thermal inertia and traversability (lower thermal inertia, worse traction; and vice versa). Another key behavior is noticed for vegetated soils, where a similar thermal inertia to wet sand is obtained but with only a third of moisture content. These results may be considered for maximizing traversability over sandy soils with higher thermal inertias, what eventually means higher compaction and safer routes. To the authors' knowledge, this is the first work addressing the correlation between moisture content and vegetation, and the thermal properties of a soil using a light-weight thermal camera that can be mounted on a mobile robot.

Thermal vision, moisture content, and vegetation in the context of off-road mobile robots

Ramón González[1,*], Alejandro López[2], Karl Iagnemma[1]

[1] *Massachusetts Institute of Technology, 77 Massachusetts Avenue, Bldg. 35, 02139, Cambridge, MA, USA*
[2] *University of Almería, Research Centre CIAIMBITAL. Ctra. Sacramento s/n, 04120 Almería, Spain*

Abstract

This paper describes an initial investigation that shows the major impact that moisture and vegetation produce on a soil and how that effect may be measured using a thermal camera. In particular, those two variables influence how the soil compacts and, hence, the traversability of a vehicle. A broad set of experiments, under different weather conditions and with different soils, demonstrate that thermal properties derived from the thermal camera (i.e. thermal inertia) increase when moisture content of sandy soils increases. In addition to that, a relation is observed between thermal inertia and traversability (lower thermal inertia, worse traction; and vice versa). Another key behavior is noticed for vegetated soils, where a similar thermal inertia to wet sand is obtained but with only a third of moisture content. These results may be considered for maximizing traversability over sandy soils with higher thermal inertias, what eventually means higher compaction and safer routes. To the authors' knowledge, this is the first work addressing the correlation between moisture content and vegetation, and the thermal properties of a soil using a light-weight thermal camera that can be mounted on a mobile robot.

Keywords: terrain traversability; terrain characterization; non-geometric hazards; thermal inertia; moisture meter; temperature probe.

*Corresponding author.
Email addresses: ramong@mit.edu (R. González), alexlopez@ual.es (A. López), kdi@mit.edu (K. Iagnemma)

1. Introduction

Mobile robots operating in off-road conditions have been successfully applied in numerous areas such as planetary exploration (Ding et al., 2011; Iagnemma & Dubowsky, 2004), agriculture (Gonzalez et al., 2009; Kondo et al., 2011), and military operations (Nath & Levinson, 2014), among others. However, what makes mobile robots interesting also makes them challenging, that is, accessing unprepared and challenging terrain (e.g. sand dunes, ripples, steep slopes), which may lead to risky situations (e.g. vehicle entrapment, high slippage, increased power consumption). While some of these "terrain-induced hazards" can be mitigated through judicious vehicle design, other issues can only be addressed through appropriate on-board control techniques (Gonzalez & Iagnemma, 2016; Gonzalez et al., 2014; Iagnemma & Dubowsky, 2004).

There is a broad body of literature dealing with control techniques for off-road mobile robots focused on the robot-terrain interaction. Many of those techniques rely on visual cameras in order to predict the traversability of the terrain in front of the robot (see Definition 1) (Chhaniyara et al., 2012; Gonzalez et al., 2016; Papadakis, 2013). The pioneering work in (Bellutta et al., 2000) describes a terrain cover color-based classification algorithm, which retrieves terrain surface characteristics by means of pattern recognition techniques. This strategy motivated the work in (Angelova et al., 2007), in which an approach to predict slip from a distance using stereo imagery is proposed. The utility of combining proprioceptive sensors (e.g. IMU and motor current) with a stereo camera to extend terrain classification from near to far distance is also demonstrated in (Bajracharya et al., 2009). Rearward-facing cameras have also been used for estimating slippage by measuring the trace produced by the wheels (Reina et al., 2010).

Even though, visual cameras have vastly demonstrated their capabilities of predicting terrain traversability, they may become insufficient when developing autonomous platforms that should operate in low-visibility conditions or in even

more challenging conditions (e.g. fog, smoke, dust). In those contexts, thermal technology means a reasonable alternative. More specifically, to the advantage of using a light-weight remote sensing device, thermal radiation can penetrate smoke and mist more readily than visible radiation. In addition to that, thermal cameras can be used for estimating physical properties of a terrain (i.e. thermal inertia). This feature is specially advisable for terrain traversability prediction in order to generate safe routes.

Although thermal imaging is still not broadly used in mobile robotics, there are some works that have successfully demonstrated its goodness. On the one hand, the work in (Caillas, 1990; Cunningham et al., 2015a,b) is framed within the context of planetary exploration rovers. Those papers relate physical properties of a soil to thermal properties derived from a thermal camera (i.e. thermal inertia). That information is then used for discriminating between fine and coarse soils. On the other hand, thermal cameras have been combined with visual cameras for improving their accuracy in low-visibility conditions (Brunner et al., 2013; Owens & Matthies, 2000).

The contribution of this paper lies in analyzing the correlation between the physical properties (i.e. moisture content and vegetation) and the thermal properties (i.e. thermal inertia) of various soils by means of a thermal camera. This work also contributes a correlation between thermal inertia and the terrain traversability, loss of traction, of a scaled vehicle. In contrast to the previous results in (Caillas, 1990; Cunningham et al., 2015a,b), terrain traversability is not only considered in terms of the grain size but also in moisture content.

This paper is organized as follows. Related work is reviewed in Section 2. Theoretical considerations dealing with thermal inertia are described in Section 3. The experimental setup is introduced in Section 4. Section 5 explains the terrain characterization. Section 6 analyzes the field tests including the temperature variation and the thermal inertia estimation. A deep discussion of field tests is addressed in Section 7. Finally, Section 8 concludes the paper and highlights future works.

Definition 1. *Terrain traversability is defined as the ability of a vehicle to assess a terrain minimizing the risk of entrapment and maximizing the mobility. In this sense, compact terrains are more traversable than deformable terrains.*

2. Related work

The two main topics of this work: the use of thermal technology for deriving physical properties of a terrain, and the influence of soil moisture and vegetation in terrain traversability comprise two broad bodies of literature.

On the one hand, satellite observations in the infrared region of the spectrum have been widely used for characterizing the Earth's surface (e.g. soil moisture) since the 1970s (Idso et al., 1975; Pratt & Ellyett, 1979; Price, 1977). In those pioneering studies, one key parameter was employed to characterize the soil surface composition, thermal inertia (see Section 3). The use of thermal vision has also shown its suitability since the 1970s with the exploration of Mars: Viking mission (Kieffer et al., 1977) and Mars Global Surveyor (Jakosky et al., 2000; Mellon et al., 2000). More recently, infrared technology was successfully employed in the MER mission by means of the Mini-TES experiment (Fergason et al., 2006). Those experiments were mainly performed for scientific reasons, that is, for understanding geologic processes occurring on Mars.

The second issue addressed in this paper, correlation between soil strength and moisture content, has been analyzed in numerous references. When a soil is completely dry it will not compact to its greatest density; however, when moisture increases, the water wets the soil allowing it to move into a more compact state (Ghosh, 2013). In contrast, when the moisture content exceeds the optimum moisture content further compaction is not possible. Water excess is even counterproductive as demonstrated in (Blahova et al., 2013; Cokca et al., 2004; Lopez et al., 2012b; Rajaram & Erbach, 1999). Those papers show that cohesion initially increases with moisture content, but when water is higher than certain values a significant drop in cohesion is observed. Another way to quantify the strength of a soil is with the known Cone Index (CI) (Wong,

2010). Research has been carried out to describe the impact of soil moisture on CI (Ayers & Perumpral, 1982; Kumar et al., 2012). Those investigations show that CI increases as water content approaches the optimum value, but it rapidly decreases when water overpasses that limit.

3. Modeling thermal inertia

Thermal inertia is a measure of the resistance of a material to changes in temperature. In the context of this paper, this thermal property is a function of: grain size, cementation (i.e. cohesion), and porosity (i.e. volume of voids) of a soil (Piqueux & Christensen, 2009). For those reasons, thermal inertia has a major impact on the compaction (Ghosh, 2013; Departments of the Army and the Air Force, 1988; Philip, 1969), and the penetration resistance of a soil (Hummel et al., 2004). Thermal inertia is defined as

$$I = \sqrt{\rho k c}, \tag{1}$$

where ρ is the bulk density, k is the thermal conductivity, and c is the specific heat of the material. Thermal inertia cannot be calculated directly and retrieving it is far from trivial. There are two traditional ways to estimate thermal inertia.

On the one hand, thermal inertia is derived by comparing the radiation temperature measurements, made in general during 24-hour heating cycles, with the temperature inferred from a thermal model. This way involves the solution of a partial differential equation of parabolic form whose surface boundary condition is non-linear and involves Drichlet and Neumann elements (Kahle, 1977; Kieffer, 2013; Mellon et al., 2000).

On the other hand, a simpler approach was proposed in the mid-1970s (Price, 1977, 1985); since then it has been employed by numerous references (Kahle, 1980, 1987; Pratt & Ellyett, 1979; Sabol et al., 2006). Here, thermal inertia (or apparent thermal inertia) is estimated by comparing temperature differences at different times of day. Typically, measurements are made near noon (T_{day})

and midnight (T_{night}) to maximize the contrast (Sabol et al., 2006). More specifically, the Apparent Thermal Inertia (ATI) is calculated as (Sabol et al., 2006)

$$I = \frac{1-A}{T_{day}-T_{night}}, \quad (2)$$

where A is the surface albedo. This equation gives I in Viking-era units $[cal\,cm^{-2}K^{-1}s^{-1/2}]$ to convert it to SI units $[Jm^{-2}K^{-1}s^{-1/2}]$ a factor of 4,186 is multiplied. The limitations of this simple approach are explained in (Price, 1985). Among others, this model may lead to inaccurate results when inter-mountain and highly irrigated regions are considered.

The use of ATI sacrifices accuracy in favor of an explicit simple formula having a straightforward physical interpretation. It bears mentioning that the solution based on the heat transfer model is not free of inaccuracies and uncertainties because of the following issues (Cunningham et al., 2015a; Fergason et al., 2006; Putzing & Mellon, 2007): (1) it requires the knowledge of various parameters that are not measurable and need to be estimated; (2) it requires numerical methods for solving the set of equations; (3) the computational cost is also considerable. For all those reasons, the ATI model, Eq. (2), is used in this work for estimating thermal inertia. In any case, the values of thermal inertia obtained in this paper are quite similar to those values obtained in similar conditions using the more complicated model (Cunningham et al., 2015a; Putzing, 2006; Sabol et al., 2006).

4. Experimental setup

Field experiments were performed on a testing site built for this particular occasion. Three main issues were raised during the building process: (1) scalable and modular configuration where various soils can be tested; (2) comfortable arrangement able to manage easily the bulky and heavy soil sacks required to fill the bins; (3) accessible disposition able to place cameras, sensors, and all the computing elements required.

Figure 1 shows the testing site developed by the authors in Almeria (Spain). Four bins with four representative soil types were first assembled. Those containers have dimensions of 1 [m] wide, 1 [m] length, and 0.5 [m] depth. These dimensions were determined after reviewing several studies dealing with terrain characterization. In those studies, the maximum penetration was normally less than 0.5 meters, see for example (Wong, 2001) and the references therein. Soils were cleaned, dried, and sieved, before being stored in the bins. The four soils mean a broad range of soil properties and, hence, different thermal properties are obtained. Soils are further detailed in Section 5. It is important to point out that no compaction process was applied to the soil bins; thus, compaction is only due to gravity and moisture content (in the wet-sand bin).

A second configuration of the testing site was also under investigation. This configuration is displayed at the top left corner of Figure 1. Here, the wet- and dry-sand bins were replaced by a vegetated soil bin (barley) and a new sand bin. In addition to that, an artificial lighting system was installed to light/heat the surfaces at night. The main features of this lighting system are: power 500 [W], height 1.5 [m], and hours of operation from 12 am to 8:30 am.

4.1. Sensors and hardware

In order to have a general knowledge of the thermal and weather conditions available during the experiments and for validating the temperatures measured by the thermal camera, a broad set of sensors were installed in the testing site. It bears mentioning that all the sensors have been replicated for redundancy and fault tolerance, this explains the broad set of sensors used here (24 sensors). The sampling period for all the sensors was 1 minute. Some of the sensors used can be seen in Figure 1.

As detailed in Table 1, various temperature probes were submerged in each soil bin for measuring the temperature at approximately 0.01 [m] below the surface. Two weather stations measuring atmospheric temperature, relative humidity, and wind speed were placed in opposite sides of the soil bins for redundancy. All the signals generated in this testing site were monitored by

Figure 1: Testing site specifically built for these experiments. Notice the modular and scalable configuration of the soil bins as well as the accessible disposition of the place for setting sensors and hardware. Observe, at the top left corner, the second configuration of this testing site with a soil bin with grass (top right corner) and the artificial lighting system used at night

means of four data loggers (Campbell Scientific, CR3000), and two laptops (Dell Precision M2300, Intel Core 2 Duo, 2.50 GHz, 4 GB). All the sensors are sold by Campbell Scientific, but the wind sensor was sold by Gill.

4.2. Thermal and visual cameras

The key component of the testing site is the thermal camera. In this case, the compact 1.4-kg infrared camera ThermoVision A40-M of the company FLIR Systems is employed. This thermal camera has a spectral infrared range of 7.5 to 13 μm, a temperature range of -40 to 120 [deg, C], and an accuracy of $\pm$ 2%. The detector is a focal plane array, uncooled microbolometer of 320 $\times$ 240

Table 1: Main features of the sensors used to monitor thermal and weather conditions in the testing site

Sensor	Model	Units / Place	Features
Temperature probe	T-108	8 / 2 for each soil bin	range: -5 to 95 deg C, tolerance: ±0.2 deg C
Averaging soil thermocouple probe	T-CAV	3 / 1 for each soil bin (except bedrock)	range: -270 to 300 deg C
Moisture meter	CS616	2 / dry and wet sand bins	range: ± 0.7 V square wave, accuracy: ± 2.5 %, resolution: 0.1 %
Pyranometer	SP1110	2 / 1 for each weather station	range: 0 to 1,750 W/m^2, accuracy: ± 5 %
Temperature and relative humidity probe	CS215	2 / 1 for each weather station	humidity: range: 0 to 100 %, accuracy: ± 2%, resolution: 0.03 %; temperature: range: -40 to 70 deg C, accuracy: ± 0.3 deg, resolution: 0.01 deg
Ultrasonic wind sensor	Windsonic	2 / 1 for each weather station	range: 0-60m/s, wind direction: 0-359 deg, accuracy: ±2% at 12m/s, resolution: 0.01m/s

pixels and a field of view of 24 × 18 degrees. The thermal sensitivity is of 0.08 degrees at 30 [deg, C]. The image processing software used for operating the camera is ThermaCAM Researcher Pro 2.8 SR-3. In this case, images are taken every minute (period = 1 minute).

In addition to the thermal camera, a visual camera has been placed in the testing site (Logitech QuickCam Sphere). This camera is synchronized with the thermal camera, which allows to understand better the thermal images. The software for recording video with this camera was WebcamXP.

Figure 2 displays the four soil bins during the first configuration of the testing site (tags: bedrock, wet sand, gravel, dry sand) at 3pm, which means the time when the temperature difference is larger. Observe the temperature differences between the soil bins. The element in the middle, tagged as “Silverpaper”, was used for calculating the background radiation level (Lopez et al., 2012a).

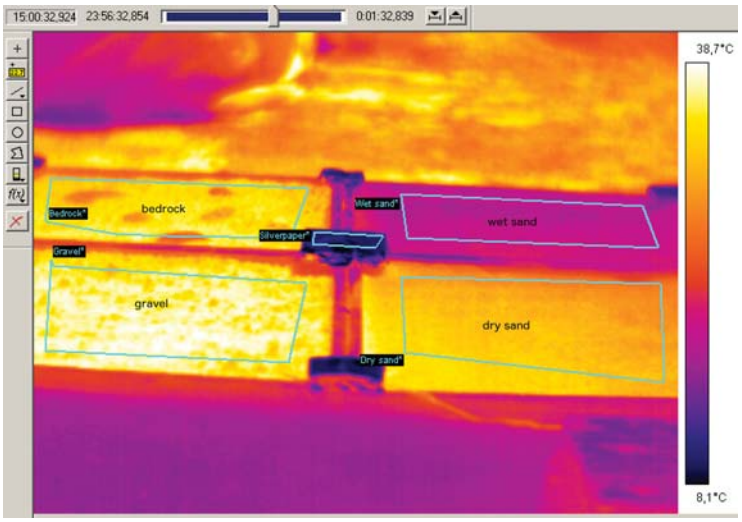

Figure 2: Thermal view of the first configuration of the testing site. Notice that at 3 pm the hottest sample is gravel and the coldest is wet sand

5. Terrain characterization

This section addresses the terrain characterization step performed before running the experiments with the thermal camera. Observe that three sets of measurements have been collected in order to properly characterize the soil bins considered in this work. Those experiments were run according to two official European Standards: UNE-EN 933-1:2012 and UNE 103900:2013. The last section addresses a quantitative analysis of terrain traversability.

It bears mentioning that the experiments addressed in the first subsection, sieving method, have been performed in a laboratory (gradation test). The experiments described in the next subsection, nuclear method, were conducted in the testing site, see Figure 3d.

5.1. Determination of particle size distribution. Sieving method

The sieving method or gradation test constitutes a common procedure in civil engineering. It describes the engineering properties of a soil based on the size of the particles, the amounts of the various sizes and the characteristics of

the very fine grains. The result of the sieving method is provided in terms of a graph of percent passing versus the sieve size, this gives the type of gradation of the soil. This gradation of the soil can be used for classifying the soil. In this case, the Unified Soil Classification System (USCS) has been used for that purpose (Holtz & Kovacs, 1981; U.S. Department of Defense, 1985).

The results obtained are plotted in Figure 3. As observed, gravel and sand represent poor graded soils, that is, they have aggregate of approximately the same size. The curve on the gradation graph is very steep and occupies a small range of the aggregate. In contrast, bedrock constitutes a well graded soil composed of equal amounts of various sizes of aggregate. This explains the even curve on the gradation graph. In gravel, 97% of the samples are retained between the 12.5-mm and 5-mm sieves. This also explains why gravel has very little fine aggregate particles (less than 1% are smaller than 4 [mm]). According to this result, this soil can be classified, following USCS, as: poorly graded gravel (GP). Sand shows a similar result to that previously mentioned, poorly graded soil, but now the samples are trapped in smaller sieves. In particular, 94% of the samples are smaller than 2 [mm]. This soil can be classified as: poorly graded sand (SP). Finally, bedrock is composed of a wide range of particle sizes and has a good representation of all sizes starting from 10 [mm] to 0.063 [mm]. For that reason, this soil is classified as: well-graded sand (SW).

5.2. Determination of density and moisture content. Nuclear methods

With the purpose of determining the density and moisture content that are going to be considered as ground-truth in this work a fairly accurate device has been employed: a nuclear density meter. This device uses a radioactive isotope source that emits photons (usually Gamma rays) which radiate back to the meters detectors at the bottom of the unit. Dense soil absorbs more radiation than loose soil and the readings reflect overall density. Water content can also be measured following that procedure (Multiquip Inc., 2012).

Table 2 shows the moisture content and density of the six soils measured with the nuclear meter. It bears mentioning that in this case the probe was

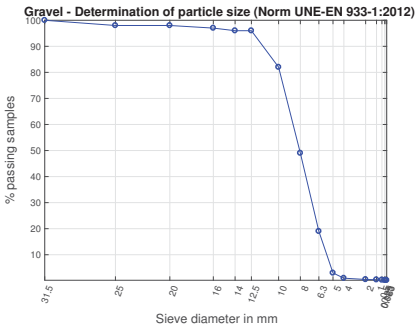

(a) Gravel. USCS: Poorly graded gravel (GP)

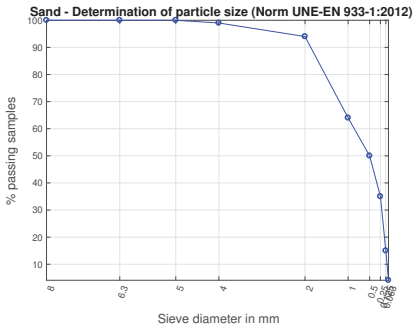

(b) Sand. USCS: Poorly graded sand (SP)

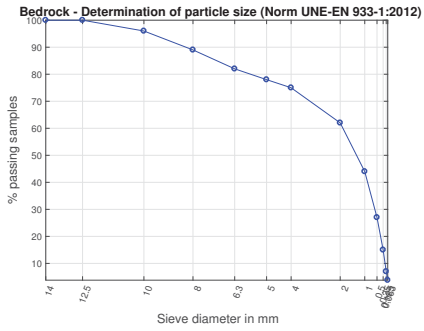

(c) Bedrock. USCS: Well-graded sand (SW)

(d) Nuclear density meter

Figure 3: Sieve results after passing the soil samples through the column of sieves. Notice the narrow or uniform gradation of gravel and sand and the dense gradation of bedrock. The nuclear meter is also displayed during operation on the testing site

nailed down at a depth of 0.3 [m] (recall that the depth of the soil bins is 0.5 [m]).

Observe that "dry" sand has a moisture content of 3.96%. This is not altogether unexpected because in nature the air contains water vapor and it is then almost impossible to achieve a moisture content of 0% in sand specially at a depth of 0.3 [m]. In any case, notice that the dry density of dry sand and wet sand is different; this result was expected because in the same volume less particles (less mass) is present in wet sand than in dry sand as the air voids are filled with water. As previously explained, bedrock represents a well-graded soil,

it leads to a dense structure because small particles fill the voids in the large particles. This structure explains why bedrock achieves the highest density. In addition to that, bedrock shows a certain moisture content, 1.68%, because it is partially composed of dry sand. The density of gravel is quite similar to dry sand, this is explained because even though the particles are larger than sand, there are air voids between particles. This increases the volume but reduces the mass.

Table 2: Density and moisture content obtained with the nuclear meter at a depth of 0.3 [m]

sample	moisture content (%)	wet density (kg/m^3)	dry density (kg/m^3)
dry sand	3.96	1.66	1.59
wet sand	19.10	1.58	1.32
sand	12.01	1.60	1.45
bedrock	1.68	1.87	1.84
gravel	0.23	1.60	1.59
grass	6.01	1.64	1.55

5.3. Traversability study

This last section addresses the compaction of the soil bins and the mobility of a vehicle on each soil bin. It bears mentioning that several methods have been evaluated for measuring the compaction of the soil, among others: Proctor compaction test and standard penetration test (Multiquip Inc., 2012). However, those methods require large machinery (e.g rollers, rammers) and are only used in large civil-engineering tasks (e.g. roads, buildings, etc.). This has prevented us from finding a laboratory with the proper equipment for the relatively small soil bins assembled here ($1 \times 1 \times 0.5\,[m^3]$).

Keeping in mind the small dimensions of the soil bins, which avoids the use of a full-size vehicle or robot, traversability was "quantified" by measuring the time that a scaled vehicle moved from two opposite corners in a soil bin. This way to quantify traversability is based on the loss of traction induced by slippage. This "loss of traction" eventually implies a higher time reaching a

target position. More specifically, the time required to travel from A to B is higher as slip increases and is infinite when slip is 100%.

The vehicle used in these experiments was an RC car, which weights 0.43 [kg] and has pneumatic tires with a tread pattern. For each test, the RC car moved at a constant velocity by pulling the trigger in the transmitter to maximum power (full-throttle). The vehicle moved six times on the same bin. The traveling time was normalized following a known approach: $x' = (x - x^m / x^M - x^m)$, where x^m, x^M are the minimum and maximum values, respectively. In this case, the absolute traveling times varied between 1 and 5 [s], and the traveled distance was 0.9 [m].

Table 3 shows the traveling time of the scaled vehicle for each soil bin. The best "traversability", less loss of traction, was observed in wet sand where the vehicle experienced neither slippage nor sinkage. A similar result was obtained in the sandy bin with a moisture content of around 12%. Gravel meant a proper mobility but a bumpy ride that sometimes led to embedding events. Bedrock caused some embedding events when the wheels moved over loose dry sand. Because of the cohesionless nature of the dry-sand bin (surface), the vehicle got stuck in all the experiments.

Observe that the grass bin has been excluded from this comparison. It was difficult to test the scaled vehicle with the vegetated terrain because the plants were taller than the wheels of the vehicle and it got trapped. In any case, it has been previously demonstrated that the presence of vegetation in sandy soil means the soil is stabilized and leads to an efficient traversability of full-scale vehicles (Department of the Army, 1994). For that reason, the vegetated-soil bin has been considered the second best scenario in this work after wet sand.

Table 3: Traveling time for each experiment. Notice that the columns show the traveling time normalized between 0-1; being 0 the case when the vehicle needs 1 [s] to travel 0.9 [m], and 1 when it requires 5 [s]

soil bin / test number	#1	#2	#3	#4	#5	#6	norm. time
dry sand	∞	∞	∞	∞	∞	∞	∞
wet sand	0.02	0	0	0	0	0.02	0.01
sand	0	0.12	0.20	0	0	0.20	0.09
bedrock	0.52	0.30	0.50	0.52	0.72	0.95	0.59
gravel	0.77	1	0.27	0.50	0.52	0.80	0.64

6. Results

This section describes the field tests performed to measure the evolution of the surface temperature and to derive thermal inertia. The first four sections analyze the experiments in terms of the temperature measured by the thermal camera and the other variables measured with the sensors and weather stations. After that, the apparent thermal inertia is estimated, while considering the procedure described in Section 3, and it is related to moisture content and traversability.

The following emissivity values have been considered in this work (Wolfe & Zissis, 1985): dry sand 0.92, wet sand 0.95, gravel 0.90. The value for bedrock has been obtained taking into account the mixed composition of this bin (dry sand and rocks), eventually, a value of 0.93 has been selected. The emissivity of grass has been selected as 0.98, according to the authors' experience for similar vegetated terrains (Lopez et al., 2012a). Another key element related to the calculation of thermal inertia is the albedo. According to the Kirchhoff's law of thermal radiation for an arbitrary body emitting and absorbing thermal radiation in thermodynamic equilibrium, the emissivity is equal to the absorptivity. This result leads to the following relation: $A = 1 - \epsilon$, where A is albedo and ϵ is emissivity (Wolfe & Zissis, 1985).

Finally, it bears mentioning that the surface temperature derived from the

thermal camera has been obtained as the average value of the whole surface of the soil bin (see rectangles in Figure 2).

An interesting video showing a 24-hour cycle of thermal and visual images is available at: `http://web.mit.edu/mobility/videos/thermal_camera_24hour.mp4`.

6.1. Experiment 1. Clear sunny day

Figure 4a shows the surface temperatures obtained using the thermal camera. Observe a typical 24-hour cycle where the temperature drops and then increases one hour after sunrise (7am). After that, the temperature increases and drops again at dusk. This plot demonstrates the key role of moisture content in the variation of the temperature. In fact, the body with the smallest variation is the wet-sand bin. Observe, in Figure 4c, that the wet sand has a moisture content between 15-20% during this 24-hour cycle. Special mention must be made of the fact that moisture content has been kept within the desired threshold by manual watering.

It bears mentioning that the highest differences among the soils appear from 10 am to 8 pm. This means the capacity of discrimination is mostly valid during the day.

Figure 4b shows that the difference dry-wet sand is high during the day because water cools the surface of the wet-sand bin. It is not altogether unexpected to see that the difference between dry sand and bedrock is very small because bedrock is mainly composed of fine sand. Gravel is always hotter than dry sand. There are two key factors that might explain this result: (1) wind cools more easily the small grains of sand than the small stones of gravel; (2) gravel is composed of almost black stones and sand is composed of bright tiny grains. As demonstrated in (Wolfe & Zissis, 1985), dark materials mean a smaller reflectivity (or higher absorptivity), and hence, they get warm more easily. Finally, gravel is always hotter than bedrock because the (bright) rocks in the bedrock bin are colder than the smaller stones in gravel.

The temperatures obtained with the probes submerged in the bins are displayed in Figure 4d. These results validate the temperature profiles obtained with the thermal camera. Obviously, slight differences are observed because those probes are submerged at 0.01 [m] below the surface. In particular, different dynamics and heat fluxes may occur (evaporation, wind, humidity, etc.).

Finally Figures 4e, 4f deal with weather variables: relative humidity, wind speed, solar irradiance, and air temperature. These plots demonstrate that this experiment was performed during a mild day with moderate wind speeds (0.4 - 2.8 [m/s]), and a clear day with no clouds: solar irradiance from 0 to 1,000 [W/m^2] and from 1,000 to 0 [W/m^2] with no significant disturbances.

6.2. Experiment 2. Cloudy and rainy day

Figure 5a displays the result during a rough day with cloudy periods and a heavy rain and strong wind during the central part of the day. This experiment demonstrates that the temperature measured with the thermal camera (top layer) is always higher than the temperature of the subsurface when there is a high sun irradiance (clear sky), see Figure 5d. However, when the sun is not shining (clouds and rain) the temperature of all the soil bins becomes similar, see Figure 5b. When the sun heats the bins after the rain, there is again a noticeable difference in the surface temperatures. A similar behavior is observed regarding the temperature of the sensors submerged in the soils.

An interesting behavior appears regarding the moisture content of both the wet-sand and dry-sand bins. Notice that even though it is raining from 12 pm to 3 pm the moisture content does not change, see Figure 5c. Recall that the moisture meters are at a depth of 0.2 [m] and perhaps the rain water evaporates at the surface of the bins. Even in the case of the wet sand, moisture drops until the human waters again at 3:30 pm. As in the previous experiment, a constant moisture content is ensured by manually watering the bin.

Finally, Figures 5e, 5f show the weather measurements. Especial mention is for Figure 5f where solar irradiance and temperature drops suddenly from 12 pm to 3:30 pm, that is, when the rainy event happened.

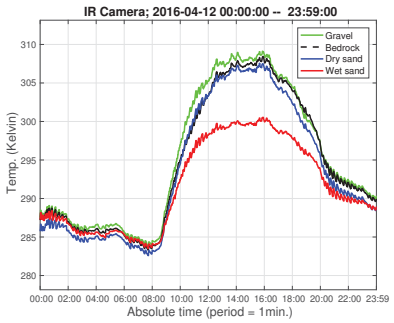

(a) Surface temperature with thermal camera

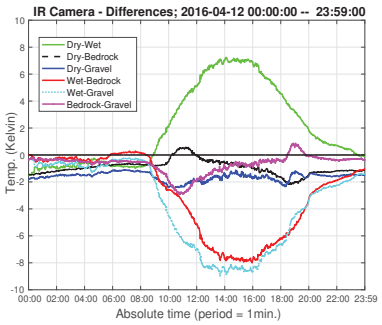

(b) Difference between camera temperatures

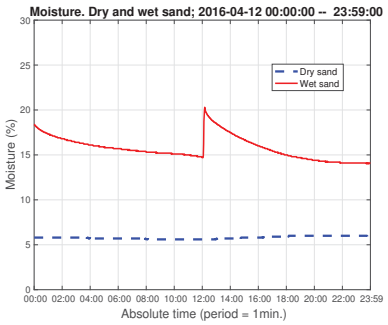

(c) Moisture content of sand bins

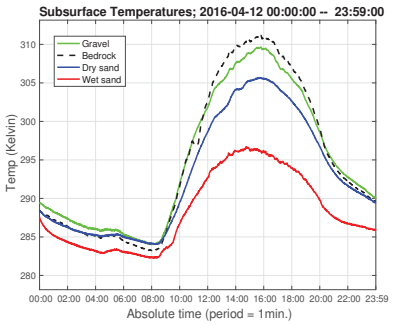

(d) Subsurface temperature with sensors

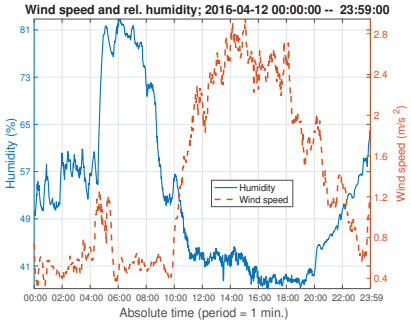

(e) Wind speed and relative humidity (weather station)

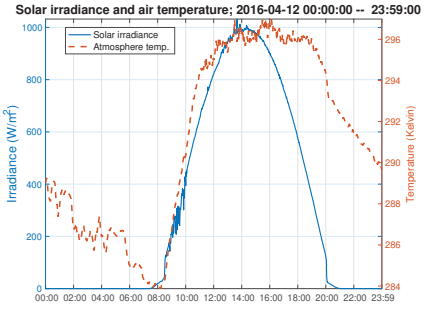

(f) Solar radiation and atm. temperature (weather station)

Figure 4: Experiment 1. Clear sunny day. Observe the major difference between the surface temperatures is in the morning and afternoon

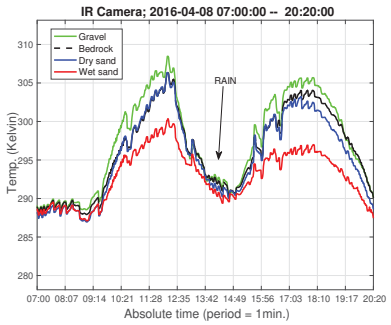

(a) Surface temperature with thermal camera

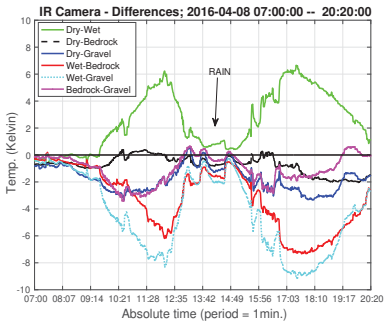

(b) Difference between camera temperatures

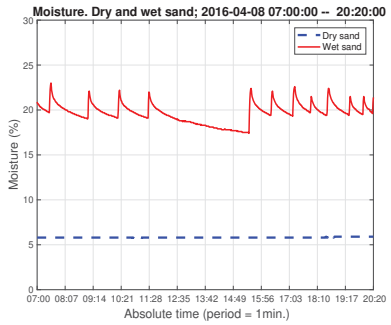

(c) Moisture content of sand bins

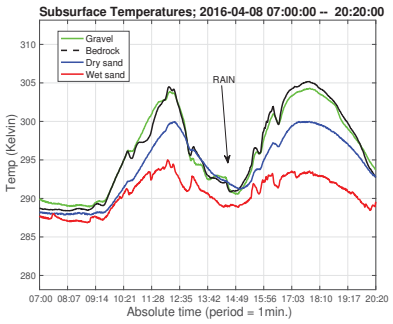

(d) Subsurface temperature with sensors

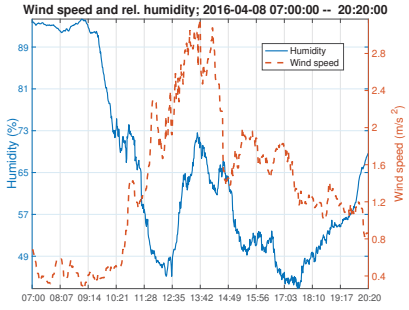

(e) Wind speed and relative humidity (weather station)

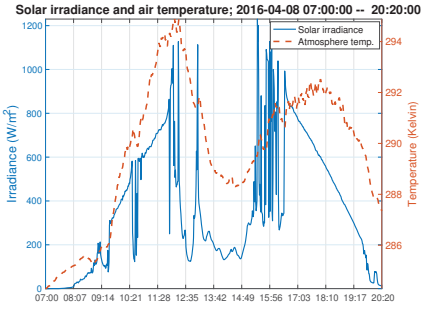

(f) Solar radiation and atm. temperature (weather station)

Figure 5: Experiment 2. Cloudy and rainy day. Notice that during the cloudy period the surface temperatures becomes similar.

6.3. Experiment 3. Vegetated soil and artificial lighting system

This experiment is based on the second configuration of the testing site (grass, sand, gravel, bedrock). Additionally, the artificial lighting system previously described was switched on at night.

Figure 6 shows the behavior of the different soil bins during a 48-hour cycle. The first conclusion is that the temperature of the grass is similar to the profile observed in the wet-sand bin in previous experiments. However, two key variables are different here, the first one is that now a much hotter day is considered (irradiance $> 1,000$ $[W/m^2]$), and the second difference is that the moisture content of grass is almost one third of the one in wet sand (7% versus 20%). This result shows that vegetation cools a surface much more efficiently than water. Notice that some studies show that there is a correlation between the density of plants (leaf area index, LAI) and soil moisture (Liu et al., 2016). However, it is difficult to generalize such relation because it depends on several factors (e.g. atmospheric variables) and even on the soil type.

Another interesting conclusion is drawn after switching on the lighting system at night, see Figures 6a, 6b, 6c. Notice that the temperatures of the soil bins during the second night are slightly higher under similar weather conditions, Figure 6e, 6f. In any case, this difference is not big enough to ensure that this change is due to the lighting system, perhaps because the lamp was far from the bins (> 1.5 $[m]$).

6.4. Experiment 4. Using an artificial heating system at night

This last experiment intends to show if it is possible to discriminate the soils considered in this work at night. Recall that, after sunset the difference between the surface temperatures is small enough that prevents the discrimination between soils using the thermal camera.

Figure 7a shows the way to proceed in this experiment. Each soil bin is lit for 2 minutes with a 500-W artificial lighting system at a distance of 1 [m] approximately. Figure 7b shows the result for the second configuration of the testing site (grass, gravel, sand, bedrock). Observe that the surface temperature

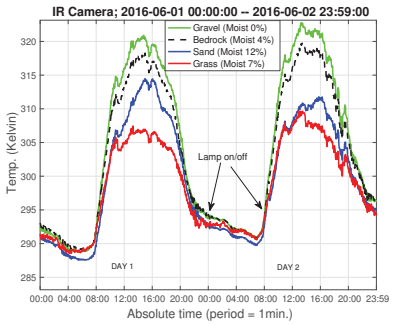

(a) Surface temperature with thermal camera

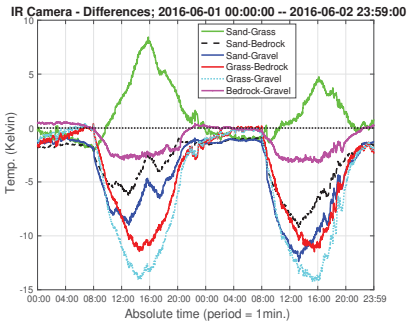

(b) Difference between camera temperatures

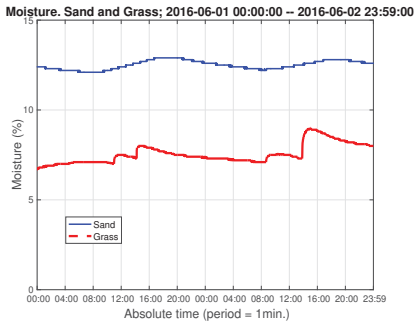

(c) Moisture content of sand and grass

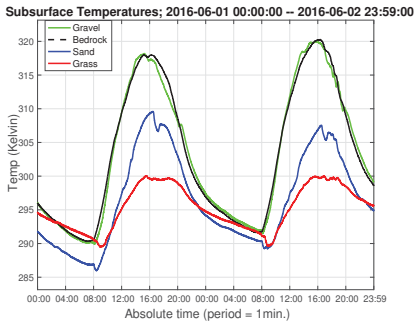

(d) Subsurface temperature with sensors

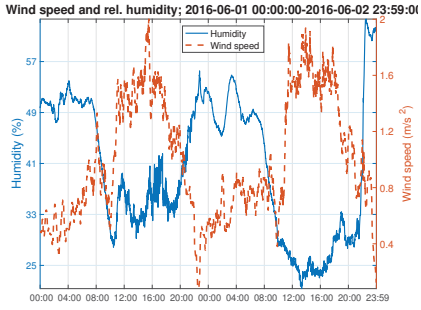

(e) Wind speed and relative humidity (weather station)

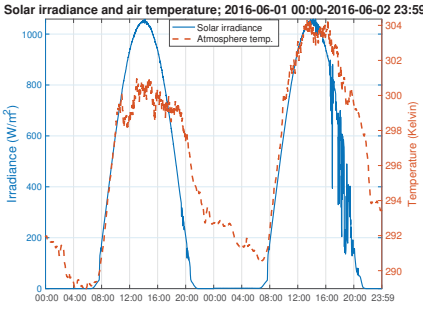

(f) Solar radiation and atm. temperature (weather station)

Figure 6: Experiment 3. Vegetated soil and artificial lighting system

actually changes when it is heated by the lighting system. In particular, grass and bedrock change around 1 degree, and sand and gravel around 0.5 degrees. It bears mentioning that the change between measurements due to noise in the sensor is much smaller than these values (0.1-0.2 degrees).

This simple experiment demonstrates that there is a certain correlation between the heating time and the increment in the soil temperature, which may be used for discriminating soils. In any case, an improved lighting/heating system will be analyzed in the future together with the following variables: distance between the lighting system and the soils, the power of the lamp, and the exposure time.

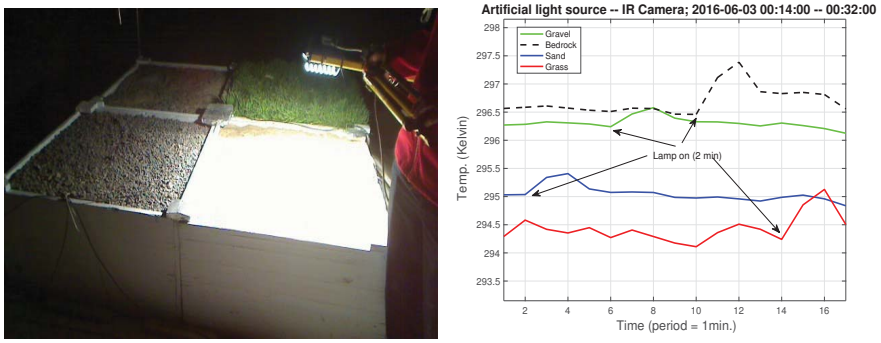

(a) Artificial lighting system (b) Surface temperature with thermal camera

Figure 7: Experiment 4. Heating a surface at night with an artificial lighting system. Observe that surface temperatures actually vary during the 2-minute exposure time

6.5. Correlation between thermal inertia, moisture, and traversability

This last section deals with the main contributions of this paper, that is, the influence of soil moisture and vegetation on thermal inertia, and the relation between thermal inertia and traversability (based on the metrics detailed in Section 5.3).

Figure 8a shows thermal inertia estimated for the sandy soils in relation to moisture content. Observe that even though all these surfaces are composed of the same basic material (i.e. sand), thermal inertia increases with soil moisture.

A remarkable behavior is obtained with the vegetated soil. In this case, a similar thermal inertia to wet sand is obtained even though the moisture content is almost one third of wet sand.

Recall that thermal inertia is related to the compaction of a surface, and compaction with traversability. Traversability comprises a key variable for controlling a mobile robot in off-road conditions. In this context, Figure 8b constitutes the second major contribution of this paper. Observe that there is a relation between traversability and thermal inertia. In addition to that, this result shows that the surfaces with the highest thermal inertia, wet sand and grass, also mean the most traversable/compact terrains. Recall that high traversability implies low embedding risk (i.e. low slippage) and poor traversability may lead to untraversable routes (i.e. high slippage).

7. Discussion

Heat and moisture fluxes from the surface to the atmosphere are controlled by turbulent transfer processes which depend on various factors: wind speed, surface roughness, atmospheric temperature, and relative humidity, among others (Price, 1985). Because of the complexity of this process and the limitations of estimating thermal inertia from thermal vision this paper does not aim to contribute a quantitative and accurate method for discriminating soils. However, this paper does contribute a proper methodology for using lightweight thermal cameras (onboard vehicles) to identify those soils where thermal inertia is higher than others, which may mean a higher moisture content and a superior traversability.

This paper demonstrates that discrimination between wet-sand, dry-sand, and vegetated areas is possible by means of thermal vision. Dry sand deals with cohesionless soils (no water wetting the soil). Due to this loose nature, dry sand is usually avoided as there is a high risk of vehicle entrapment. On the other hand, wet sand and vegetation would probably imply more compact soils, higher cementation, and hence, more appropriate for robot motion. However, it

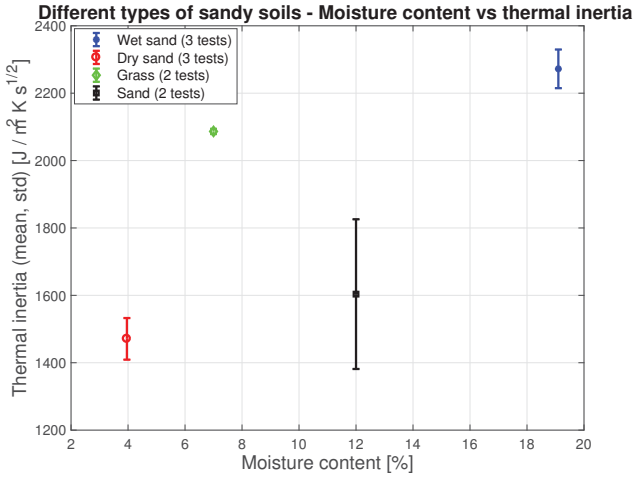

(a) Thermal inertia versus moisture content for the sandy soils

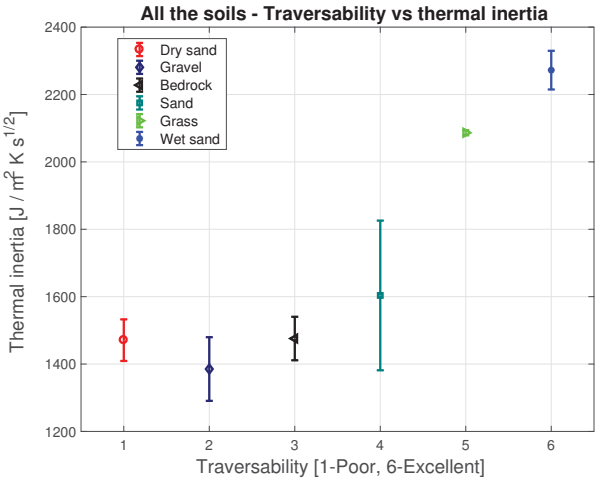

(b) Thermal inertia versus traversability

Figure 8: Quantitative analysis of thermal inertia. Observe the relation between thermal inertia and moisture content, and between thermal inertia and traversability (poor traversability means high slippage, and excellent traversability implies no slippage)

is also important to remark that when the moisture content of a soil is up to the optimum moisture content (or maximum dry density) of such soil, compaction is

adversely influenced (Ghosh, 2013). This fact highlights that thermal signature or thermal inertia maybe is not enough to identify the optimal compact state of wet sand. In any case, future research will be performed with a broader set of moisture levels (from dry sand to mud) to validate the previous statement.

As observed in the previous experiments, discrimination between soils is only advisable during the day. Recall that at night the temperature difference between the soil bins is almost zero. More specifically, the difference is within 2 degrees from 12 am to 8 pm. This result highlights an important controversy to the traditional advantage of thermal cameras, that is, night operation. For that reason, a second set of experiments have been carried out using an artificial lighting system. This preliminary solution shows that discrimination between soils can be achieved by means of a trade-off between the power of the artificial lighting system, the exposition time, and the distance to the soil.

8. Conclusions and future work

Thermal cameras constitute a remarkable perception system for off-road mobile robots and autonomous ground vehicles. This paper means an initial investigation focused on the challenges associated with the use of thermal cameras in wet and vegetated soils, and shows how thermal properties actually depends on the moisture content and the relation between those thermal properties and traversability. As a proof of concepts, traversability is understood in terms of the loss of traction and the traveling time of a scaled vehicle moving over the soil bins.

This paper benefits from the simple model that estimates the apparent thermal inertia. In any case, future research will concentrate on solving the more complicated heat transfer model as well as validating the derived thermal inertia with ground-truth values. In addition to that, future efforts will address the determination of thermal inertia over short periods of time (e.g. 1 minute or 2 minutes) instead of the current 24-hour cycle. That research will benefit from the preliminary results obtained here with the artificial lighting system

with 2-minute cycles.

Observe that one key limitation of the use of thermal cameras for terrain traversability is that they detect features associated with the upper few centimeters of a surface. However, terrain traversability is also dictated by the layer below the topmost terrain surface. In this sense, thermal cameras may be complemented with other sensors (e.g. ground penetrating radars).

Finally, a comprehensive analysis will be run in order to determine the traversability of an actual vehicle moving over the considered soils. This step will enable closed-loop control of mobile robots in off-road conditions predicting terrain traversability by means of a thermal camera.

9. Acknowledgements

The authors would like to acknowledge the assistance of more than 10 individuals who participated in the construction of the testing site, especial mention for E. Sanchez, and Prof. D.L. Valera from the University of Almeria (Almeria, Spain). The research described in this publication was carried out at the University of Almeria (Spain) and at the Massachusetts Institute of Technology (USA), under the STTR Contract NNX15CA25C funded by NASA.

References

Angelova, A., Matthies, L., Helmick, D., & Perona, P. (2007). Learning and Prediction of Slip from Visual Information. *Journal of Field Robotics*, *24*, 205–231.

Ayers, P., & Perumpral, J. (1982). Moisture and Density Effect on Cone Index. *Transactions of the ASAE*, *25*, 1163 – 1172.

Bajracharya, M., Howard, A., Matthies, L., Tang, B., & Turmon, M. (2009). Autonomous Off-Road Navigation with End-to-End Learning for the LAGR Program. *Journal of Field Robotics*, *26*, 3–25.

Bellutta, P., Manduchi, R., Matthies, L., Owens, K., & Rankin, A. (2000). Terrain Perception for DEMO III. In *IEEE Intelligent Vehicles Symposium* (pp. 326 – 331).

Blahova, K., Sevelova, L., & Pilarova, P. (2013). Influence of Water Content on the Shear Strength Parameters of Clayey Soil in Relation to Stability Analysis of a Hillside in Brno Region. *Acta Universitatis Agriculturae et Silviculturae Mendelianae Brunensis*, *61*, 1583 – 1588.

Brunner, C., Peynot, T., Vidal-Calleja, T., & Underwood, J. (2013). Selective Combination of Visual and Thermal Imaging for Resilient Localization in Adverse Conditions: Day and Night, Smoke and Fire. *Journal of Field Robotics*, *30*, 641 – 666.

Caillas, C. (1990). *Thermal Imaging for Robotic Applications in Outdoor Scenes*. Technical Report CMU-R1-TR-90-08 Carnegie Mellon University.

Chhaniyara, S., Runskill, C., Yeomans, B., Matthews, M., Saaj, C., Ransom, S., & Richter, L. (2012). Terrain Trafficability Analysis and Soil Mechanical Property Identification for Planetary Rovers: A Survey. *Journal of Terramechanics*, *49*, 115 – 128.

Cokca, E., Erol, O., & Armangil, F. (2004). Effect of Compaction Moisture Content on the Shear Strength of a Unsaturated Clay. *Geotechnical and Geological Engineering*, *22*, 285 – 297.

Cunningham, C., Nesnas, I., & Whittaker, W. (2015a). Terrain Traversability Prediction by Imaging Thermal Transients. In *IEEE Int. Conf. on Robotics and Automation (ICRA)* (pp. 3947 – 3952). Seattle, Washington: IEEE.

Cunningham, C., Wong, U., Peterson, K., & Whittaker, W. (2015b). Predicting Terrain Traversability from Thermal Diffusivity. In L. Mejias, P. Corke, & J. Roberts (Eds.), *Field and Service Robotics* number 105 in Springer Tracts in Advanced Robotics (pp. 61 – 74). Springer.

Department of the Army (1994). *Planning and Design of Roads, Airfields, and Heliports in the Theater of Operations – Road Design. Ch. 7. Soils Trafficability*. Field Manual FM 5-430-00-1 US Army Washington, DC, USA.

Departments of the Army and the Air Force (1988). *Artic and Subartic Construction-Calculation Methods for Determination of Depths of Freeze and Thaw in Soils*. Technical Report TM 5-852-6 US Department of Defense.

Ding, L., Deng, Z., Gao, H., Nagatani, K., & Yoshida, K. (2011). Planetary Rovers' Wheel-Soil Interaction Mechanics: New Challenges and Applications for Wheeled Mobile Robots. *Intelligent Service Robotics*, *4*, 17–38.

Fergason, R., Christensen, P., Bell, J., Golombek, M., Herkenhoff, K., & Kieffer, H. (2006). Physical Properties of the Mars Exploration Rover Landing Sites as Inferred from Mini-TES-derived Thermal Inertia. *Journal of Geophysical Research*, *111*, 1 – 18.

Ghosh, R. (2013). Effect of Soil Moisture in the Analysis of Undrained Shear Strength of Compacted Clayey Soil. *Journal of Civil Engineering and Construction Technology*, *4*, 23 – 31.

Gonzalez, R., & Iagnemma, K. (2016). Soil Embedding Avoidance for Planetary Exploration Rovers. In *8th ISTVS Amercias Conference*. Detroit, MI, USA: International Society for Vehicle-Terrain Systems.

Gonzalez, R., Rituerto, A., & Guerrero, J. (2016). Improving Robot Mobility by Combining Downward-Looking and Frontal Cameras. *Robotics*, *[In Press]*.

Gonzalez, R., Rodriguez, F., & Guzman, J. L. (2014). *Autonomous Tracked Robots in Planar Off-Road Conditions. Modelling, Localization and Motion Control*. Series: Studies in Systems, Decision and Control. Springer, Germany.

Gonzalez, R., Rodriguez, F., Sanchez-Hermosilla, J., & Donaire, J. (2009). Navigation Techniques for Mobile Robots in Greenhouses. *Applied Engineering in Agriculture*, *25*, 153–165.

Holtz, R., & Kovacs, W. (1981). *An Introduction to Geotechnical Engineering*. Prentice-Hall, USA.

Hummel, J., Ahmad, I., Newman, S., Sudduth, K., & Drummond, S. (2004). Simultaneous Soil Moisture and Cone Index Measurement. *Transactions of the ASAE*, *47*, 607 – 618.

Iagnemma, K., & Dubowsky, S. (2004). *Mobile Robots in Rough Terrain. Estimation, Motion Planning, and Control with Application to Planetary Rovers*. Springer Tracts in Advanced Robotics. Springer, Germany.

Idso, S., Schmugge, T., Jackson, R., & Reginato, R. (1975). The Utility of Surface Temperature Measurements for the Remote Sensing of Surface Soil Water Status. *Journal of Geophysical Research*, *80*, 3044 – 3049.

Jakosky, B., Mellon, M., Kieffer, H., Christensen, P., Varnes, E. S., & Lee, S. (2000). The Thermal Inertia of Mars from the Mars Global Surveyor Thermal Emission Spectrometer. *Journal of Geophysical Research*, *105*, 9643 – 9652.

Kahle, A. (1977). A Simple Thermal Model of the Earth's Surface for Geologic Mapping by Remote Sensing. *Journal of Geophysical Research*, *82*, 1673 – 1680.

Kahle, A. (1980). Remote Sensing in Geology. chapter Surface Thermal Properties. (pp. 227 – 273). John Wiley & Sons, USA.

Kahle, A. (1987). Surface Emittance, Temperature, and Thermal Inertia Derived from Thermal Infrared Multispectral Scanner (TIMS) Data for Death Valley, California. *Geophysics*, *52*, 858 – 874.

Kieffer, H. (2013). Thermal Model for Analysis of Mars Infrared Mapping. *Journal of Geophysical Research*, *118*, 451 – 470.

Kieffer, H., Martin, T., Peterfreund, A., & Jakosky, B. (1977). Thermal and Albedo Mapping of Mars During the Viking Primary Mission. *Journal of Geophysical Research*, *82*, 4249 – 4291.

Kondo, N., Monta, M., & Noguchi, N. (2011). *Agricultural Robots. Mechanisms and Practice*. Kyoto University Press.

Kumar, A., Chen, Y., Sadek, A., & Rahman, S. (2012). Soil Cone Index in Relation to Soil Texture, Moisture Content, and Bulk Density for No-tillage and Conventional Tillage. *Agricultural Engineering International CIGR Journal*, *14*, 1 – 16.

Liu, L., Zhang, R., & Zuo, Z. (2016). The Relationship between Soil Moisture and LAI in Different Types of Soil in Central Eastern China. *Journal of Hydrometeorology*, *16*.

Lopez, A., Molina-Aiz, F., Valera, D., & Peña, A. (2012a). Determining the Emissivity of the Leaves of Nine Horticultural Crops by means of Infrared Thermography. *Scientia Horticulturae*, *137*, 49 – 58.

Lopez, E., Herrera, M., Gonzalez, O., Tijskens, E., & Ramon, H. (2012b). Determination of the Basics Mechanical Properties in a Tropical Clay Soil as a Function of Dry Bulk Density and Moisture. *Revista Ciencias Tecnicas Agropecuarias*, *21*, 5 – 11.

Mellon, M., Jakosky, B., Kieffer, H., & Christensen, P. (2000). High-Resolution Thermal Inertia Mapping from the Mars Global Surveyor Thermal Emission Spectrometer. *Icarus*, *148*, 437 – 455.

Multiquip Inc. (2012). *Soil Compaction Handbook*. Multiquip Inc., USA.

Nath, V., & Levinson, S. (2014). *Autonomous Military Robotics*. SpringerBriefts in Computer Science. Springer, Germany.

Owens, K., & Matthies, L. (2000). Passive Night Vision Sensor Comparison for Unmanned Ground Vehicle Stereo Vision Navigation. In *IEEE Int. Conf. on Robotics and Automation (ICRA)* (pp. 122 – 131). San Francisco, CA, USA: IEEE volume 1.

Papadakis, P. (2013). Terrain Traversability Analysis Methods for Unmanned Ground Vehicles: A Survey. *Engineering Applicatons of Artificial Intelligence*, *26*, 1373 – 1385.

Philip, J. (1969). Theory of Infiltration. *Advances in Hyroscience*, *5*, 215 – 296.

Piqueux, S., & Christensen, P. (2009). A Model of Thermal Conductivity for Planetary Soils: 2. Theory of Cemented Soils. *Journal of Geophysical Research*, *114*, 1–12.

Pratt, D., & Ellyett, C. (1979). The Thermal Inertia Approach to Mapping Soil Moisture and Geology. *Remote Sensing of Environment*, *8*, 151 – 158.

Price, J. (1977). Thermal Inertia Mapping: A New View of the Earth. *Journal of Geophysical Research*, *82*, 2582 – 2590.

Price, J. (1985). On the Analysis of Thermal Infrared Imagery: The Limited Utility of Apparent Thermal Inertia. *Remote Sensing of Environment*, *18*, 59 – 73.

Putzing, N. (2006). *Thermal Inertia and Surface Heterogeneity on Mars*. Ph.D. thesis Colorado School of Mines Golden, Colorado, US.

Putzing, N., & Mellon, M. (2007). Apparent Thermal Inertia and the Surface Heterogeneity of Mars. *Icarus*, *191*, 68 – 94.

Rajaram, G., & Erbach, D. (1999). Effect of Wetting and Drying on Soil Physical Properties. *Journal of Terramechanics*, *36*, 39 – 49.

Reina, G., Ishigami, G., Nagatani, K., & Yoshida, K. (2010). Odometry Correction using Visual Slip Angle Estimation for Planetary Exploration Rovers. *Advanced Robotics*, *24*, 359 – 385.

Sabol, D., Gillespie, A., & Mcdonald, E. (2006). Differential Thermal Inertia of Geological Surfaces. In J. Sobrino (Ed.), *Int. Symposium on Recent Advances in Quantitative Remote Sensing*. Valencia, Spain: Global Change Unit, University of Valencia.

U.S. Department of Defense (1985). Annual Book of ASTM Standards. D 2487-83, 04.08 chapter Classification of Soils for Engineering Purposes. (pp. 395 – 408). American Society for Testing and Materials.

Wolfe, W., & Zissis, G. (Eds.) (1985). *The Infrared Handbook*. (Second ed.). Ann Arbor. The Univiersity of Michigan Press, USA.

Wong, J. (2001). *Theory of Ground Vehicles*. (Third ed.). John Wiley & Sons, Inc., USA.

Wong, J. (2010). *Terramechanics and Off-Road Vehicle Engineering*. (Second ed. ed.). Butterworth-Heinemann (Elsevier).